# Nonlinear response of a neoclassical four-field magnetic reconnection model to localized current drive

E. Lazzaro[1], L. Comisso[1], and L. Valdettaro[2]

[1]*Istituto di Fisica del Plasma CNR, Euratom-ENEA-CNR Association,*

*Via R. Cozzi 53, 20125 Milan, Italy*

[2]*Department of Mathematics, Politecnico di Milano,*

*Piazza L. da Vinci 32, 20133 Milan, Italy*

FP10/01 February 2010

*To be submitted for publication*

# Nonlinear response of a neoclassical four-field magnetic reconnection model to localized current drive

E. Lazzaro[1], L. Comisso[1], and L. Valdettaro[2]

[1]*Istituto di Fisica del Plasma CNR, Euratom-ENEA-CNR Association, Via R. Cozzi 53, 20125 Milan, Italy*

[2]*Department of Mathematics, Politecnico di Milano, Piazza L. da Vinci 32, 20133 Milan, Italy*

**Abstract**

In tokamaks magnetic islands arise from an unstable process of tearing and reconnecting of helical field lines across rational surfaces. After a linear stage the magnetic instability develops through three characteristic nonlinear stages where increasingly complex topological alterations occur in the form of the magnetic islands . The problem of response of reconnection process to the injection of an external current suitably localized is addressed using a four-fields model in a plane slab plasma, with a novel extension to account consistently of the relevant neoclassical effects, such as bootstrap current and pressure anisotropy. This finding has implications on the interpretation of the possible mechanism of present day experimental results on NTMs as well as on the concepts for their control or avoidance.

PACS numbers: 52.55Fa, 52.55.Tn, 52.35.Py, 52.35.Vd

## I. INTRODUCTION

The contemporary research in the physics of tokamak plasmas is strongly focussed towards the task of controlling the most serious instabilities, associated with dissipative magnetohydrodynamics (MHD) [1,2]. Among the most striking phenomena to be considered foremost are the instabilities of magnetic reconnecton where the breaking and the rejoining of magnetic field lines that are closed, leads to dramatic changes in topology of the closed magnetic configuration where the plasma is held in equilibrium, with detrimental effects. In a tokamak the nested isobaric confinement surfaces are "torn" in subdomains called magnetic islands that grow in time, eroding the plasma profiles. The magnetic reconnection process is ubiquitous in plasma physics and has been widely studied both in laboratory and in astrophysics environments, but in high temperature tokamak plasmas specific aspects need being considered, in the regimes of low collisionality and important toroidal effects, called "neoclassical". In particular these aspects are important in the study of means to counteract the tearing modes instabilities by localized injection of external control current to balance the destabilising perturbations [3,4]. This approach relies on the possibility of driving current by absorption of electromagnetic wave power and many new theoretical problems arise for a consistent treatment of this new effect in the dynamics of the process. In this paper is presented an appropriate new formulation of the governing nonlinear equations for four continuum fields (magnetic flux, pressure, velocity and vorticity) in the relevant neoclassical regime. In Section II the neoclassical fluid model is reconsidered and cast in an appropriate new form extending the classical four field approach [5], to be solved numerically. In Section III the system behaviour is analysed in paradigmatic cases that are useful to address basic questions of control strategy.

## II. PHYSICS MODEL AND NUMERICAL METHOD

The dynamics of the process is described by the Maxwell equations and the plasma response given by the essential fluid equations, which consist of the generalized Ohm's law:

$$\underline{E}+\underline{v}_e\times\underline{B}=-\frac{1}{en}\underline{\nabla}p_e-\frac{1}{en}\underline{\nabla}\cdot\underline{\underline{\Pi}}_{e\|}+\eta\underline{J} \tag{1}$$

the shear-Alfvén law:

$$\underline{B}\cdot\underline{\nabla}\times m_i n\left(\frac{\partial}{\partial t}+\underline{v}_i\cdot\underline{\nabla}\right)\underline{v}_i=\underline{B}\cdot\underline{\nabla}\times\left(\underline{J}\times\underline{B}\right)-\underline{B}\cdot\underline{\nabla}\times\underline{\nabla}\cdot\underline{\underline{\Pi}} \tag{2}$$

the evolution of ion parallel velocity:

$$\hat{b}\cdot m_i n\left(\frac{\partial}{\partial t}+\underline{v}_i\cdot\underline{\nabla}\right)\underline{v}_i=-\hat{b}\cdot\underline{\nabla}p-\hat{b}\cdot\underline{\nabla}\cdot\underline{\underline{\Pi}} \tag{3}$$

and the electron mean pressure evolution equation:

$$\frac{3}{2}\left(\frac{\partial}{\partial t}+\underline{v}_e\cdot\underline{\nabla}\right)p_e+\frac{5}{2}p_e\underline{\nabla}\cdot\underline{v}_e=-\underline{\underline{\Pi}}_e:\underline{\nabla}\underline{v}_e-\underline{\nabla}\cdot\underline{q}_e+\eta J^2 \tag{4}$$

We point out here that symbols with subscript $\|(\perp)$ indicate the component parallel (perpendicular) to the magnetic field $\underline{B}$. The electric field is denoted, as usual, by $\underline{E}$, while the current density is $\underline{J}=(\underline{\nabla}\times\underline{B})/\mu_0$, with $\mu_0$ the free-space permeability, $n$ is the particle number density, $e$ is the electron charge, $\eta$ is the plasma resistivity and $\hat{b}=\underline{B}/B$. Moreover, $m_s$, $\underline{v}_s$, $\underline{q}_s$, $p_s$, $\underline{\underline{\Pi}}_s$, are respectively the mass, flow velocity, heat flux density, mean pressure and viscous stress tensor of particle species $s$. The total mean pressure is $p\equiv p_e+p_i=p_e(1+\tau_T)$, with $\tau_T$ the ion/electron temperature ratio. Similarly the total viscous stress tensor is $\underline{\underline{\Pi}}\equiv\underline{\underline{\Pi}}_e+\underline{\underline{\Pi}}_i$.

From the system (1)-(4) a neoclassical four-field model of magnetic reconnection is developed under the assumption of axisymmetric torus geometry with large aspect ratio (i.e. $\varepsilon\equiv a/R_0\ll 1$, where $a$ is the torus minor radius and $R_0$ is the torus major radius of the magnetic axis) and within a FLR-drift ordering ($v\sim\delta v_{th}$ and $\partial/\partial t\sim\delta^2\omega_c$, where $\delta\equiv\rho_L/L_\perp=\omega_{th}/\omega_c\ll 1$ is the magnetization parameter, and $v_{th}$, $\omega_{th}$, $\omega_c$, $\rho_L$, $L_\perp$ are respectively the thermal velocity, the thermal transit frequency, the cyclotron frequency, the cyclotron radius and the perpendicular characteristic scale length of the plasma).

The stress tensor terms in the equations bring in the influence of neoclassical physics; the damping of poloidal flow due to $\hat{b}\cdot\underline{\nabla}\cdot\underline{\underline{\Pi}}_i$ and the parallel electron stress tensor contributions to the Ohm's law, namely in the form of bootstrap current density and trapped electron increase of electrical resistivity $\propto\hat{b}\cdot\underline{\nabla}\cdot\underline{\underline{\Pi}}_e$. These are of crucial importance for tearing instabilities driven by perturbations of the bootstrap current density on and near the magnetic surfaces threaded by closed field lines (with rational winding number).

We develop the model starting from the viscous stress tensor written as $\underline{\underline{\Pi}}=\underline{\underline{\Pi}}_\|+\underline{\underline{\Pi}}_\wedge+\underline{\underline{\Pi}}_\perp$, where the parallel stress tensor, valid in low collisionality regimes, within the drift ordering and with small finite pressure anisotropy [6,7] $p_\Delta\equiv p_\|-p_\perp\sim\delta p$, is taken in the CGL form [8]:

$$\underline{\underline{\Pi}}_\|=(p_\|-p_\perp)\left(\hat{b}\hat{b}-\frac{1}{3}\underline{\underline{I}}\right) \tag{5}$$

The perpendicular and gyroviscous terms for the particle species $s$ are of order $\nu_s \rho_{Ls}^2 \propto \delta_s^3$ (where $\nu_s$ is the Coulomb collision frequency) but play a role in the perpendicular energy transport and in the advective terms of the ion momentum equation through the so called gyroviscous cancellation (see, e.g., Ref [9] and references therein).

The divergence of the CGL ion pressure tensor (composed from the scalar plus parallel traceless part) provides important terms for the equation of ion parallel velocity (3) and the evolution of parallel vorticity (2). After lengthy but straightforward manipulation we may write:

$$\underline{\nabla} \cdot \left( p \underline{\underline{I}} + \underline{\underline{\Pi}}_{\parallel} \right) = \underline{\nabla} p_{\perp} + \underline{B} \nabla_{\parallel} \left( \frac{p_{\Delta}}{B} \right) + p_{\Delta} \underline{\kappa} \tag{6}$$

where $\underline{\kappa} \equiv \hat{b} \cdot \underline{\nabla} \hat{b}$ is the magnetic field curvature. The parallel projection of the divergence of the CGL electron stress tensor gives origin to the neoclassical bootstrap current density in the generalized Faraday-Ohm's law in the form:

$$J_{bs} = -L_{bs} \frac{B_{\varphi}}{B B_{\theta}} \frac{\partial}{\partial r} p_e \left( 1 + \tau_T \right) \tag{7}$$

where $B_{\varphi}$ and $B_{\theta}$ are the toroidal and poloidal magnetic field components respectively, $r$ is the minor radius of the flux surface, and $L_{bs}$ is the bootstrap current single coefficient, that is expressed in terms of the elements of the neoclassical viscous and friction matrices [7,10] $\underline{\underline{\mu}}^e$ and $\underline{\underline{l}}^{ei}$.

In a reduced MHD ordering the continuum fields are represented in terms of scalar stream functions $\psi$ (poloidal magnetic flux function per radian in $\varphi$) and $\phi$ (electrostatic potential):

$$\underline{B} = B_{\varphi} \hat{e}_{\varphi} + \frac{\hat{e}_{\varphi}}{R} \times \underline{\nabla} \psi \tag{8}$$

$$\underline{v}_i = \underline{v}_{i\parallel} \hat{b} + \frac{1}{B} \hat{b} \times \underline{\nabla} \phi + \frac{1}{enB} \hat{b} \times \underline{\nabla} \cdot \left( p_i \underline{\underline{I}} + \underline{\underline{\Pi}}_{i\parallel} \right) + O\left( \delta^2 \right) \tag{9}$$

$$U = \hat{b} \cdot \underline{\nabla} \times \underline{v}_i \tag{10}$$

Considering also the electron mean pressure field, the reduced neoclassical MHD system is obtained in the form of four nonlinear PDEs, that can be developed operating in a simplified (slab) geometry, while retaining the essential physical ingredients. With the closure assumption (consistent with equation (4) and suitable for the problems addressed below) that all energy input ($\approx \eta J^2$) is balanced by heat transport loss mechanisms, the neoclassical four-field model obtained is the follow:

$$\frac{\partial \psi}{\partial t} + \frac{1}{B_0} \{ \phi, \psi \} = \frac{1}{enB_0} \{ p_e, \psi \} - \eta_{NC} \left( J_{\parallel} - J_{bs} - J_{CD} \right) + \mu_e \nabla^2 J_{\parallel} \tag{11}$$

$$\frac{\partial U}{\partial t}+\frac{1}{B_0}\{\phi,U\}=\frac{1}{m_i n}\{J_{\parallel},\psi\}+\frac{\mu_0(1+\tau_T)}{m_i n B_0^2}\left(J_{\parallel}\{\psi,p_{e\Delta}\}+p_{e\Delta}\{\psi,J_{\parallel}\}\right)+\mu_{\perp}\nabla^2 U \tag{12}$$

$$\frac{\partial v_{i\parallel}}{\partial t}+\frac{1}{B_0}\{\phi,v_{i\parallel}\}=\frac{(1+\tau_T)}{m_i n B_0}\left(\{\psi,p_e\}+\frac{2}{3}\{\psi,p_{e\Delta}\}\right)+\mu_{\parallel}\nabla^2 v_{i\parallel} \tag{13}$$

$$\frac{\partial p_e}{\partial t}+\frac{1}{B_0}\{\phi,p_e\}=\frac{1}{B_0}\left(\frac{5}{3}p_e+\frac{4}{9}p_{e\Delta}\right)\{\psi,v_{i\parallel}-J_{\parallel}/en\} \tag{14}$$

where $\{A,B\}\equiv\hat{e}_z\cdot\underline{\nabla}A\times\underline{\nabla}B$ are the Poisson brackets, $B_0$ is the toroidal magnetic field magnitude on the magnetic axis, $\eta_{NC}$ is the neoclassical resistivity [7], $\mu_e$, $\mu_{\perp}$, $\mu_{\parallel}$ are small viscosity terms arising from the development of the perpendicular viscous stress tensor, and $J_{CD}$ represents an externally driven current density (see Appendix A). Furthermore, $J_{\parallel}=\nabla^2\psi/\mu_0$ and $U=\nabla^2\phi/B_0$.

The full neoclassical model need to be closed by a constitutive relation for the pressure anisotropy. The closure adopted here was derived from neoclassical transport theory [7] and is similar to that suggested by Gianakon, Kruger and Hegna [11]:

$$p_{e\Delta}=\frac{\nu_e m_e n\mu_{00}^e q}{\varepsilon}\frac{B_0}{\langle\{\psi,B\}\rangle}\left(\frac{\partial\phi}{\partial x}-\frac{1}{en}\frac{\partial p_e}{\partial x}+\frac{1}{3en}\frac{\partial p_{e\Delta}}{\partial x}\right) \tag{15}$$

Here the operator $\langle\ \rangle$ denotes the flux-surface average [6] and $q=rB_{\varphi}/R_0B_{\theta}$ is the safety factor in the large aspect ratio circular tokamak.

We solve the dimensionless form of system of equations (11)-(15) (see Appendix B) in a two-dimensional periodic box $L_x\times L_y$, using a Fourier pseudospectral method for the space variables and a second-order Adams-Bashford method for the time variable. Production runs were carried out with a $N_x\times N_y$ grid of $200\times200$ points. The time step ($\Delta t=2\cdot10^{-3}$) was estimated using the relation [12] $\Delta t<1/\left(\max\left(N_x,N_y\right)\|u\|a\right)$, where $\|u\|$ is the perturbation norm and $a$ is the multiplicative factor of the term to be estimated. We impose the equilibrium configuration $\psi^{(0)}=\cos x$, $\phi^{(0)}=v_{i\parallel}{}^{(0)}=p_e{}^{(0)}=p_{e\Delta}{}^{(0)}=0$, and $L_x=\pi$, with the resonant surface at $x=0$. The chosen equilibrium is tearing unstable to linear perturbations of the tipe $\delta F=\mathrm{Re}\left(F_L(x)e^{\gamma t+iky}\right)$. Instability occurs at long wavelengths, such that $k=m\varepsilon_L<1$, where $m$ is the mode number and $\varepsilon_L\equiv L_x/L_y$ is the slab aspect ratio that must be less than unity [13] (in this paper we present numerical runs with $\varepsilon_L=0.5$, but the numerical study is valid for the controlled evolution of a generic $m/n$ mode). An initial perturbation is applied to the equilibrium, in the form of a small random noise on the initial conditions for the four fields.

## III. BEHAVIOR OF THE SYSTEM

The most important results of the present work are the topological configurations of the poloidal magnetic flux function, that allow us to make crucial observations about the response of a *generic* magnetic island to an external action meant to control its growth. A concise comment of paradigmatic cases is presented below, starting from the simulation of the behavior of the neoclassical model without any localized current drive.

### A. Free system

We begin presenting the results of the free system evolution starting from the time evolution of fields' spectral amplitude in the final nonlinear phase, as is illustrated in Fig. 1 (time is scaled with the Alfvén transit time). We analyse the topology evolution of poloidal magnetic flux function $\psi$ up to the stage that shows an explosive behaviour (in the absence of sufficient dissipation) of the parallel ion flow velocity and electron mean pressure fields.

Fig. 2.a show two magnetic islands on resonant surface at $t = 1800\,\tau_A$, which already after $60\,\tau_A$ appear swollen (Fig. 2.b). At $t = 1890\,\tau_A$ the evolution of the poloidal magnetic flux function has reached a stage where hyperbolic ("*X*") point collapse is followed by current sheet reconnection (Sweet-Parker stage [14,15]). When the aspect ratio of the current sheet exceeds a critical value [16], the sheet becomes unstable and generates a secondary island, as illustrated in Fig. 2.d.

It is interesting that such evolution to very small scale lengths has been previously associated to electron inertia effects [13], while here it appears to be a general feature of the nonlinearity of the problem.

### B. Localized current drive case

Three basic examples are studied numerically to characterize the nonlinear response to specific input of the external current aligned or misaligned with the magnetic island perturbation. These are organized as shown in Fig. 3, where the localization of the injected (rf) external current density $J_{CD}(\psi,t)$ (see Appendix A) is indicated (by labels 1, 2, 3) on the 2D magnetic flux map, with a developed magnetic island.

The first case (1) describes the effect of a continuous (in the island frame!) current deposition exactly centered on the island elliptic ("*O*") point, at $t = 1800\,\tau_A$ shortly after the island has appeared. If the island is rotating in the laboratory frame, this situation implies a perfect phasing

of the external source with the island. The effect of the injected current, shown in Figs. 4.a,b, is that of immediate freezing of the reconnection process and apparently a new nonlinear equilibrium state is reached and maintained with no singular elliptic and hyperbolic points, as desired. The stabilized equilibrium lasts beyond the time ($t = 1900\,\tau_A$) when the free case developed the extreme filamentation of Fig. 2.d, however, later ($t = 2100\,\tau_A$) the reconnection process starts again (Fig. 4.c) and evolves again in an irreversible nonlinear stage with hyperbolic point collapse and deformation of topology into secondary islands (Fig. 4.d).

The physics of the control process is further made clear by Fig. 5 that shows how upon application of the stabilizing $J_{CD}$, that is spread over the self-consistently varying island flux surfaces, the perturbed current, in place of the peak at the hyperbolic point, develops two current sheets on each side of the singular ($x = 0$) surface . This means that the island suppression process does not proceed through a gradual shrinking of the island size and a restoration of a state similar to the initial one, but settles on the alternative equilibrium, without reconnection in a magnetic island but with current sheets, well known from fundamental theoretical expectations [17,18]. This result is a non trivial cause of concern for the validity of control strategies that are *customarily* proposed, based on the concept of a gradual effect on the island evolving essentially self-similarly, and on estimates of the helical current injection by continuous (synchronous) application of rf power on the "*O*" point, neglecting the *self-consistent* change of the equilibrium state. Furthermore the nonlinear equilibrium reached, may be prone to further instabilities, associated with the uncontrolled and unobservable degrees of freedom.

As matter of fact the final nonlinear stage appearing in this model is characterized by the development of structures on small space scales in $x$ direction that enhance the pressure gradient to the point that the assumed ordering $p_{e\Delta} \sim \delta p_e$ may be violated and, in absence of sufficient loss mechanisms, the coupled equations (13) and (14) develop a finite time explosive behavior [19], as apparent in Fig. 6, setting a limit to the validity of the calculation.

The second example corresponds to $J_{CD}$ injection at point (2), with a moderate radial misalignment with respect to the elliptic point, and is shown in Figs. 7.a,b. Apparently the initial effect is similar to that of perfect centering of $J_{CD}$ on the "*O*" point, with a significant shrinking of the island effective size (Fig. 7.a) and "healing" of the "*X*" point, but the current sheets (Fig. 7.b), do not screen fully the driven current filaments. Therefore even a moderate *radial* misalignment of the applied current "filament" with respect to the elliptic point *may not* succeed in the total suppression of the island and in the long run ($t \approx 2090\,\tau_A$) deteriorates irreversibly the topology with multiple secondary islands.

Finally the third case describes the most interesting situation of moderate, constant, phase misalignment of the injected $J_{CD}$ with respect to the elliptic point, as shown by (3) in Fig. 3. For an island rotating in the laboratory frame, this would correspond to an imperfect *initial* focussing of the external wave beam intercepting the island. Of course this case is the most likely to occur in practice. The result shown in Fig. 8.a is that as long as the current deposition is radially localized on the rational surface and not too close to the hyperbolic point, it provides the *same effect* of freezing the reconnection process as the perfect localization on the elliptic point. Fig. 8.b confirms that the new nonlinear equilibrium is without singular points and with current sheets replacing the island structure.

Several questions concerning the strategy of control of the Neoclassical Tearing Modes (NTMs) stability in realistic configurations can benefit from the above conclusion, albeit qualitative. Indeed the identification of (observable) state variables appears more subtle than in the conventional case that deals just with island width and frequency. It appears that the timing and an appropriate localization of the control current, related to beam focussing, cannot be done ignoring the island nonlinear shape evolution, and the fact that reconnection can be "healed" but the initial state cannot be restored since the new nonlinear equilibrium reached is irreversible. A further extension of this model, even before a formulation in realistic (toroidal) geometry, should consider various effect of energy losses, here deliberately neglected. Indeed the unstable degrees of freedom of a many-fields system, may be usefully quenched, if they cannot all be tracked (observable) and controlled.

## IV. CONCLUSIONS

An extension of the scalar field model of magnetic reconnection [5,13,16,20,21] was developed for application in the neoclassical regime where NTM instabilities appear, and the effect of an externally injected control current was studied in exemplary cases. The description of the topological and dynamical evolution of the many-fields system shows that a correct approach to define a control by current drive should consider both the self-consistent evolution of the helical equilibrium and a possible *preparation* of the dynamical system to deal with instability mechanisms hidden in variables that are hardly observable.

**ACKNOWLEDGMENTS**

This work, partially supported by the European Communities under the contract of EURATOM-ENEA-CNR Association, was carried out within the framework of EFDA. The views and opinions expressed herein do not necessarily reflect those of the European Commission. The authors gratefully acknowledges the help and support of X.J. Tian and S. Nowak.

**APPENDIX A: Current drive term**

The control current used in this work, appropriate to describe the current driven by the absorption of suitably localized rf wave power (e.g. from Electron Cyclotron wave beams), can be modelled by time dependent amplitude and a Gaussian profile of width dictated by the absorption depth $\delta_{CD}$ (a property specific of the waves considered and depending on background density, temperature, and beam propagation characteristics). After a short (parallel) thermal diffusion time $\tau_k$, much shorter than the magnetic reconnection time, a current density initially localized in close to the rational surface $r = r_s$, within a sharp angular "window" $W(\theta,\varphi)$, becomes a flux function:

$$J_{CD} = j_{CD}(t)\left( W(\theta,\varphi) e^{-\frac{(r-r_0)^2}{\delta_{CD}^2}} e^{-\frac{t}{\tau_k}} + \left(1 - e^{-\frac{t}{\tau_k}}\right) e^{-\frac{(\psi-\psi_0)^2}{\delta_{CD}^2}} \right) \xrightarrow{t \gg \tau_k} J_{CD} = j_{CD}(t) e^{-\frac{(\psi-\psi_0)^2}{\delta_{CD}^2}} \qquad (16)$$

The latter expression is used as input for the case study presented, with the dimensionless step function amplitude given by:

$$j_{CD}(t) = \begin{cases} 0 & t < 1800\,\tau_A \\ 5 & t \geq 1800\,\tau_A \end{cases}$$

and the dimensionless Gaussian function width given by $\delta_{CD}^2 = 5 \cdot 10^{-2}$.

An important observation is necessary concerning the consistency of the insertion of the rf term in the four-field system. In general the rf modifies the source terms of also equations (2)-(4) [22]. Hence, calculations of modifications to the fluid closure moments from the rf fields should follow the procedure to calculate heat fluxes and viscous stresses. However in the case of ECCD (Electron Cyclotron Current Drive), a fluid theory approach is viable as electron cyclotron wave heating and current drive do not inject momentum [23], and in the present problem it is assumed that all energy input and losses are balanced.

**APPENDIX B: Dimensionless coefficients**

The system of equations (11)-(14) can be written in dimensionless form as:

$$\frac{\partial \psi}{\partial t}+\{\phi,\psi\}=C_1\{p_e,\psi\}+C_2\left(J_{\parallel}+J_{CD}\right)-C_3\frac{\partial p_e}{\partial x}+\mu_e\nabla^2 J_{\parallel} \tag{17}$$

$$\frac{\partial U}{\partial t}+\{\phi,U\}=C_4\{\psi,J_{\parallel}\}+C_5\left(J_{\parallel}\{p_{e\Delta},\psi\}+p_{e\Delta}\{J_{\parallel},\psi\}\right)+\mu_{\perp}\nabla^2 U \tag{18}$$

$$\frac{\partial v_{i\parallel}}{\partial t}+\{\phi,v_{i\parallel}\}=C_6\left(\{\psi,p_e\}+\frac{2}{3}\{\psi,p_{e\Delta}\}\right)+\mu_{\parallel}\nabla^2 v_{i\parallel} \tag{19}$$

$$\frac{\partial p_e}{\partial t}+\{\phi,p_e\}=C_7\left(\frac{5}{3}p_e+\frac{4}{9}p_{e\Delta}\right)\{\psi,v_{i\parallel}\}-C_8\left(\frac{5}{3}p_e+\frac{4}{9}p_{e\Delta}\right)\{J_{\parallel},\psi\} \tag{20}$$

while the closure equation (15) becomes:

$$p_{e\Delta}=C_9\frac{1}{\langle\{\psi,B\}\rangle}\frac{\partial\phi}{\partial x}-C_{10}\frac{1}{\langle\{\psi,B\}\rangle}\left(\frac{\partial p_e}{\partial x}-\frac{1}{3}\frac{\partial p_{e\Delta}}{\partial x}\right) \tag{21}$$

Considering the following characteristic parameters for a tokamak plasma: $n=10^{20}\,\#/\mathrm{m}^3$, $T=10^4\,\mathrm{eV}$, $B=5\mathrm{T}$, $\tau_T=1$, $\beta=1\cdot10^{-3}$, $S=1\cdot10^3$; we obtain the dimensionless coefficients used in numerical simulations: $C_1\approx1\cdot10^{-4}$, $C_2\approx1.4\cdot10^{-3}$, $C_3\approx5\cdot10^{-5}$, $C_4=C_7=1$, $C_5=C_6=1\cdot10^{-3}$, $C_8\approx2\cdot10^{-1}$, $C_9\approx5\cdot10^{-5}$, $C_{10}\approx5\cdot10^{-7}$. Moreover, we choose the following small viscous coefficients: $\mu_e=1\cdot10^{-5}$, $\mu_{\perp}=5\cdot10^{-2}$, $\mu_{\parallel}=1\cdot10^{-4}$.

[1] A.H. Boozer, Rev. Mod. Phys. **76**, 1071 (2004).

[2] R.B. White, Rev. Mod. Phys. **58**, 183 (1986).

[3] E. Lazzaro and S. Nowak, Plasma Phys. Control. Fusion **51**, 035005 (2009).

[4] H. Zohm, Phys. Plasmas **4**, 3433 (1997).

[5] R.D. Hazeltine and J.D. Meiss, Phys. Rep. **121**, 1 (1985).

[6] F.L. Hinton and R.D. Hazeltine, Rev. Mod. Phys. **48**, 239 (1976).

[7] S.P. Hirshman and D.J. Sigmar, Nucl. Fusion **21**, 1079 (1981).

[8] G.L. Chew, M.L. Goldberger, and F.E. Low, Proc. R. Soc. London Ser. A **236**, 112 (1956).

[9] J.J. Ramos, Phys. Plasmas **12**, 112301 (2005).

[10] H. Sugama and S. Nishimura, Phys. Plasmas **9**, 4637 (2002).

[11] T.A. Gianakon, S.E. Kruger, and C.C. Hegna, Phys. Plasmas **9**, 536 (2002).

[12] A. Quarteroni, R. Sacco, and F. Saleri, *Numerical Mathematics* (Springer-Verlag, Berlin, 2006).

[13] M. Ottaviani and F. Porcelli, Phys. Rev. Lett. **71**, 3802 (1993).

[14] P.A. Sweet, in *Proceedings of the IAU Symposium 6: Electromagnetic Phenomena in Cosmical Physics* (Cambridge University Press, Cambridge, 1958), p. 123.

[15] E.N. Parker, J. Geophys. Res. **62**, 509 (1957).

[16] N.F. Loureiro, S.C. Cowley, W.D. Dorland, M.G. Haines, and A.A. Schekochihin, Phys. Rev. Lett. **95**, 235003 (2005).

[17] R.M. Kulsrud and T.S. Hahm, Phys. Scripta **T2/2**, 525 (1982).

[18] T.S. Hahm and R.M. Kulsrud, Phys. Fluids **28**, 2412 (1985).

[19] H. Wilhelmsson, E. Lazzaro, *Reaction-Diffusion Problems in the Physics of Hot Plasmas* (Institute of Physics Publishing Ltd, London, 2001).

[20] E. Lazzaro, M. Ferrero, L. Gianoli, and L. Valdettaro, Phys. Scripta **61**, 624 (2000).

[21] K.C. Schmidt, S. Günter, and K. Lackner, Phys. Plasmas **16**, 072302 (2009).

[22] C.C. Hegna and J.D. Callen, Phys. Plasmas **16**, 112501 (2009).

[23] R. Prater, Phys. Plasmas **11**, 2349 (2004).

***Figure Captions***

FIG. 1. (Color online) Time evolution of fields' spectral amplitude in the final nonlinear phase for the free system evolution case (i.e. in the absence of external current drive).

FIG. 2. (Color online) Isolines of poloidal magnetic flux function $\psi$ showing the free system magnetic island evolution. The growth of the magnetic island (a)-(b) is accompanied by the collapse of the hyperbolic point (c), and finally by the generation of a secondary island (d).

FIG. 3. (Color online) Localization of injected (rf) external current density on the 2D magnetic flux map. In the first case (1) the localized current density deposition $J_{CD}$ is exactly centered on the island elliptic point. The second case (2) corresponds to $J_{CD}$ injection with a moderate radial ($x$ direction in slab) misalignment with respect to the elliptic point. Finally the third case (3) corresponds to $J_{CD}$ injection with a moderate angular ($y$ direction in slab) misalignment with respect to the elliptic point.

FIG. 4. (Color online) Isolines of poloidal magnetic flux function $\psi$ showing the magnetic island evolution of the system with $J_{CD}$ exactly centered on the island elliptic point. The contour plots (a)-(b) show that elliptic and hyperbolic points have been erased. At $t \approx 2090\,\tau_A$ the reconnection process starts again (c), and evolves in a stage with generation of a secondary island (d).

FIG. 5. (Color online) Profile of $J_z$ when the magnetic reconnection has been forced to erase singular points by injection of (rf) external current density centered on the island elliptic point.

FIG. 6. (Color online) Time evolution of fields' spectral amplitude in the final nonlinear phase for the case of a continuous current deposition exactly centered on the island elliptic point (1). The final stage shows an explosive behavior of parallel ion flow velocity and electron mean pressure fields.

FIG. 7. (Color online) Case of $J_{CD}$ injection with a moderate radial ($x$ direction in slab) misalignment with respect to the elliptic point. Isolines of poloidal magnetic flux function $\psi$ (a) and of parallel current density (b) at $t = 1900\,\tau_A$.

FIG. 8. (Color online) Case of $J_{CD}$ injection with a moderate angular ($y$ direction in slab) misalignment with respect to the elliptic point. Isolines of poloidal magnetic flux function $\psi$ (a) and of parallel current density (b) at $t = 1900\,\tau_A$.

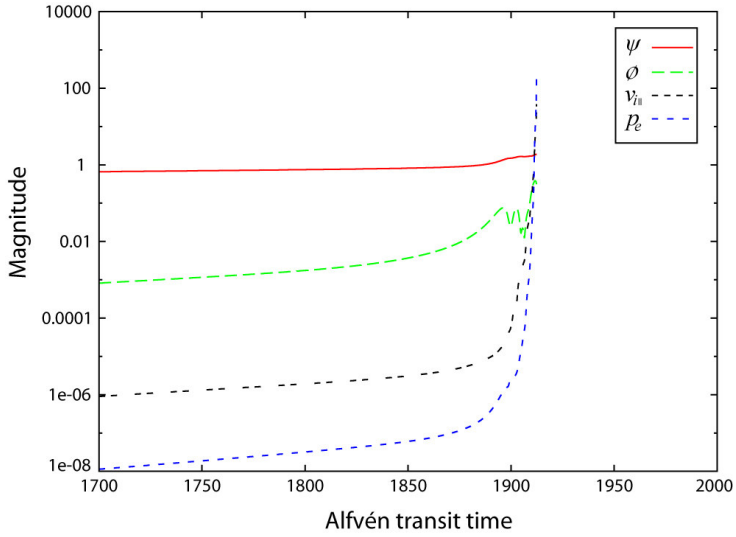


FIG. 1. (Color online)

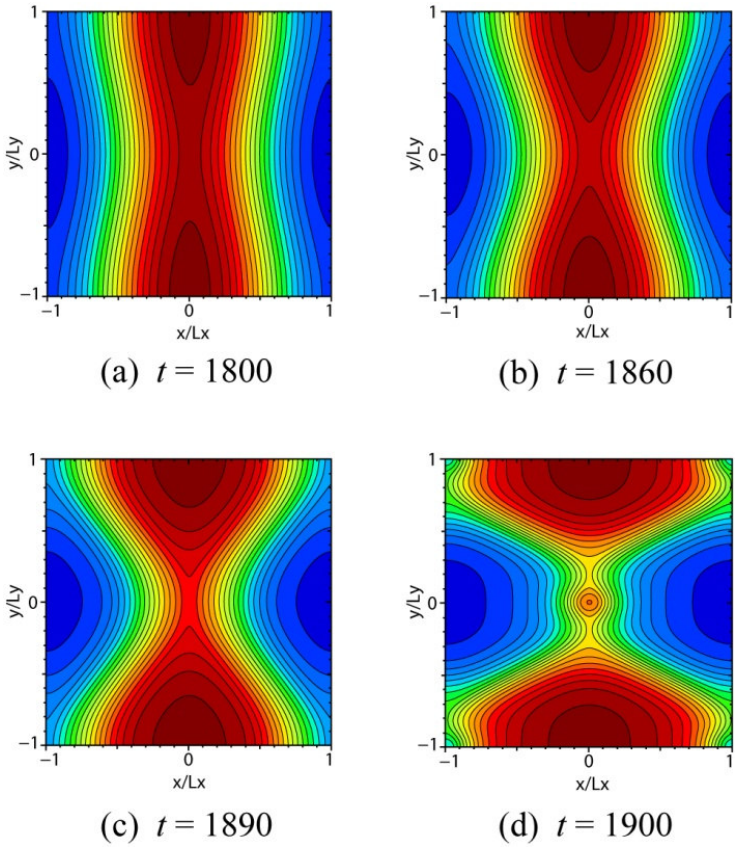


FIG. 2. (Color online)

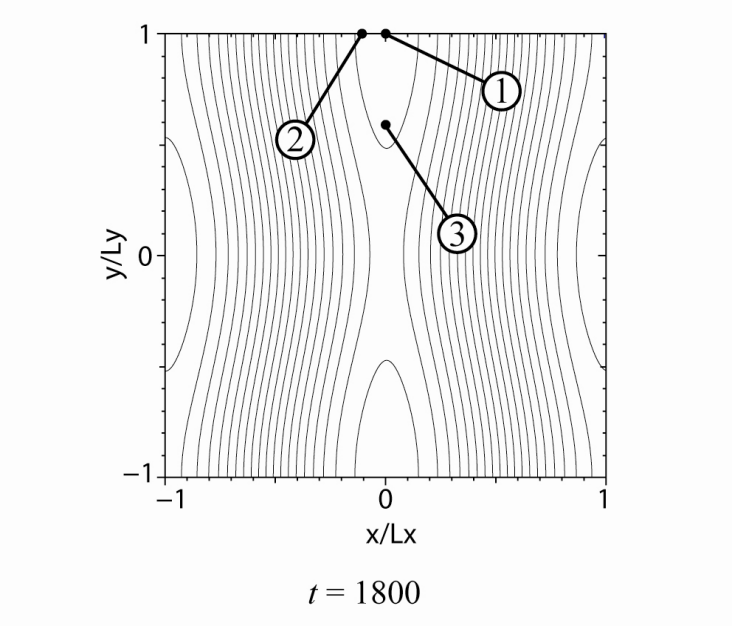


FIG. 3. (Color online)

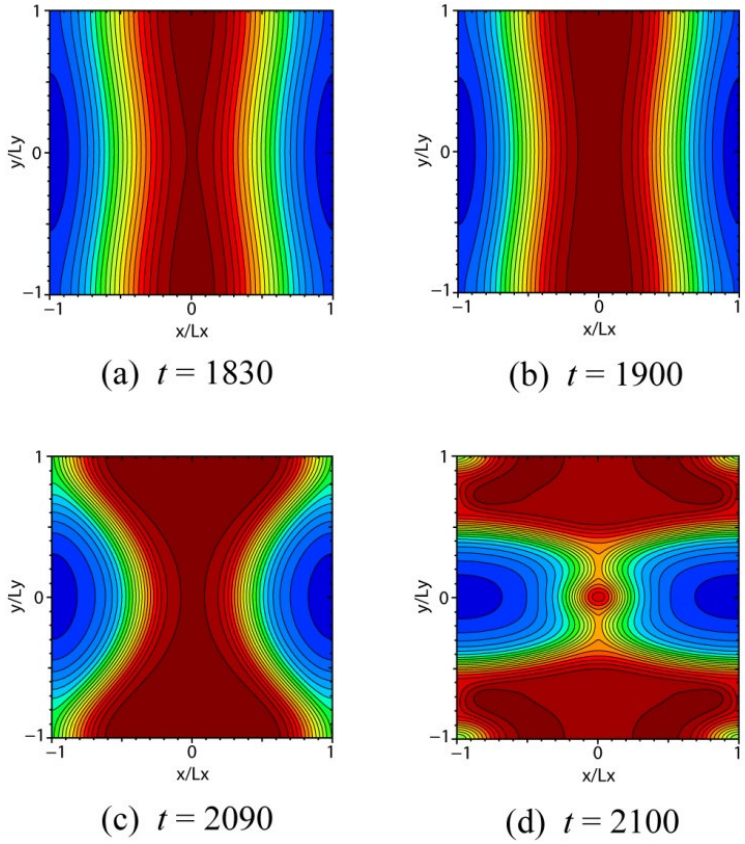


FIG. 4. (Color online)

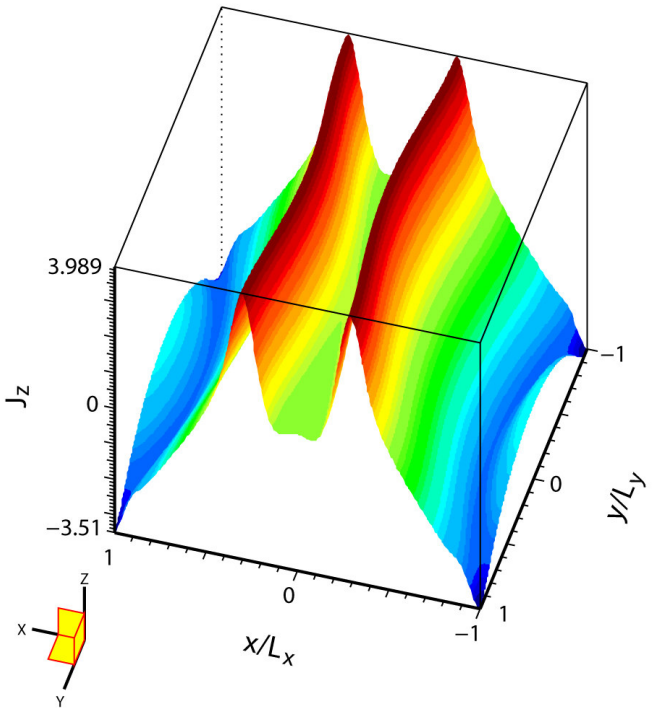


$t = 1900$

FIG. 5. (Color online)

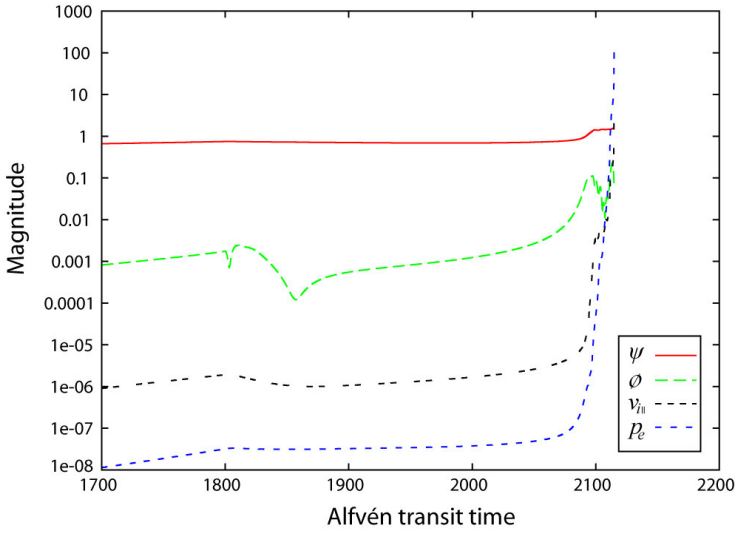


FIG. 6. (Color online)

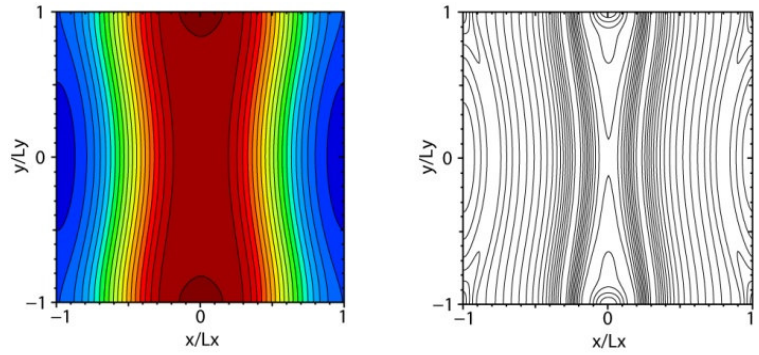


$t = 1900$

FIG. 7. (Color online)

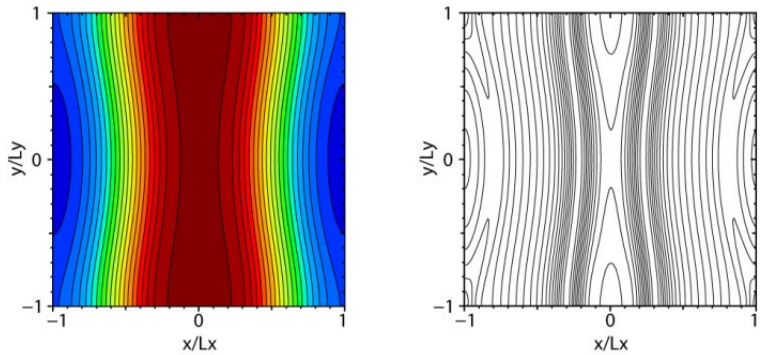


$t = 1900$

FIG. 8. (Color online)